Original Article
Bulletin of Pure and Applied Sciences
Chemistry , Vol.44 C, No.1
January-June 2025: P.31-39

http://www.bpasjournals.com/chemistry
Print version ISSN 0970 4620
Online version ISSN 2320 320X

Effect of Zinc and Strontium Doping on The Density and Hardness of Nanohydroxyapatite

Sindhu RL*

Author's Affiliations:
Assistant Professor, College of Engineering Trivandrum, APJ Abdul Kalam Technological University, Kerala 695016, India.

***Corresponding Author: Sindhu RL,** Assistant Professor, College of Engineering Trivandrum, APJ Abdul Kalam Technological University, Kerala 695016, India.
E-mail: sindhuajai8@gmail.com

ABSTRACT

Hydroxyapatite is a biocompatible, bioactive, and non-toxic bioceramic that constitutes the primary inorganic material in human bone. Synthetic hydroxyapatite is not suitable for load-bearing uses due to its insufficient mechanical strength. The mechanical properties of nano-hydroxyapatite can be improved by incorporating small amounts of trace elements that are present in bone. Zinc is found in bone at around 0.01 - 0.05 %, and strontium around 0.01 - 0.1 %. The introduction of zinc and strontium improves the properties of nanohydroxyapatite. In this study, nanohydroxyapatite and its doped samples are synthesized using a simple chemical precipitation method. The structural analysis has been done using Fourier Transform Infrared (FTIR) and X-ray diffraction (XRD) Spectroscopic techniques. The thermal properties of the synthesized sample were studied using TGA. The elemental analysis was done using EDX analysis, and the morphological analysis was done by HRTEM. The density of the sintered sample was measured using Archimedes' principle, and its Vickers hardness was also evaluated. Findings reveal that the incorporation of zinc and strontium improves the density and hardness of nanohydroxyapatite.

Keywords: Nanohydroxyapatite, Vickers hardness, Density, Zinc-doped hydroxyapatite, Strontium-doped hydroxyapatite.

Received on 22.01.2025, Revised on 31.03.2025, Accepted on 02.05.2025

How to cite this article: Sindhu R L 2025). Effect of Zinc and Strontium Doping on The Density and Hardness of Nanohydroxyapatite. *Bulletin of Pure and Applied Sciences-Chemistry,* 44C (1), 31-39.

INTRODUCTION

Hydroxyapatite (HA), $Ca_{10}(PO_4)_6(OH)_2$ is a highly regarded material that has caught the attention of researchers among various calcium phosphates due to its impressive qualities such as biocompatibility, bioactivity, osteoconductivity, non-toxicity, and anti-inflammatory properties, along with its close resemblance to the inorganic components of human bones and teeth [1-2,6]. As a result, it is frequently utilized in multiple biomedical applications, including bioactive coatings on metallic implants, middle ear implants, dental materials, tissue engineering systems, and targeted drug delivery [3]. Natural apatite crystals exhibit different properties compared to conventional synthetic hydroxyapatite. Bone crystals are formed within a biological environment through the biomineralization process. Moreover, biological

apatites exhibit non-stoichiometric compositions because they contain trace elements like magnesium, manganese, zinc, strontium, sodium, carbonates, and fluorides [4,10]. Furthermore, the bioactivity of conventional synthetic HA ceramics is not as high as that of bone. The characteristics of synthetic hydroxyapatite can be enhanced by doping it with different cations and anions. Zinc, a crucial trace element present in all biological tissues, plays a crucial role in maintaining membrane structure, protein synthesis, DNA synthesis, and cell proliferation in the human body. It also functions as an antioxidant. Hence, producing zinc-doped hydroxyapatite could be advantageous for optimizing biochemical processes [3-4,7]. Additionally, strontium (Sr^{2+}), though present in small amounts in the body, has a high bone affinity and contributes significantly to mineralization. The increasing interest in strontium-substituted hydroxyapatite (HA) for bone repair is supported by numerous studies demonstrating the beneficial effects of this element on hard tissues, such as the promotion of alkaline phosphatase (ALP), collagen type I, and increased cell proliferation. Furthermore, Sr^{2+} ions improve antiresorptive activity, enhance the solubility of the biomaterial, stimulate osteoblasts, and induce apoptosis in osteoclasts, leading to enhanced new bone formation. The biological properties of Sr^{2+} substituted HA are linked to the expansion of its crystal lattice and changes in crystallinity resulting from the differences in ionic radius [8-9].

In this work, pure nanohydroxyapatite, zinc-doped, and strontium-doped nanohydroxyapatite were synthesized using a simple chemical precipitation method, and their crystallographic properties were characterized. Doping with zinc and strontium can change the crystal structure of HA, raise lattice strain, change its solubility, and promote cell differentiation and proliferation. Zn/Sr-nHA is a promising material for enhanced bone tissue engineering, dental applications, and drug delivery systems.

MATERIALS AND METHODS

Materials

The chemicals used in this experiment are calcium nitrate tetrahydrate $Ca(NO_3)_24H_2O$, diammonium hydrogen phosphate $(NH_4)_2HPO_4$, zinc nitrate hexahydrate $Zn(NO_3)_26H_2O$ (Merck), and strontium nitrate anhydrous $Sr(NO_3)_2$. To maintain pH, ammonium hydroxide NH_4OH (99%) solution is used. All reagents were used as received.

Synthesis of pure zinc-doped and strontium-doped hydroxyapatite

Nanohydroxyapatite is synthesized using the wet chemical precipitation technique. Appropriate concentrations of calcium nitrate and diammonium hydrogen phosphate solutions are prepared and thoroughly mixed. The solution concentrations are adjusted to ensure that the Ca/P ratio consistently remains at 1.67. The calcium nitrate solution is progressively added to the diammonium hydrogen phosphate solution while stirring well. The pH of the mixture is regulated at 9 by gradually adding ammonium hydroxide solution. The resultant solution is stirred continuously for one hour and allowed to age for 12 hours. The obtained suspension is centrifuged at a speed of 4000 rpm and thoroughly rinsed with deionized water. The resulting precipitate is then heated to $80\ ^0$ C for 18 hours in a hot air oven and ground into a fine powder using an agate mortar.

To synthesize zinc-doped and strontium-doped nano-hydroxyapatite, suitable amount of zinc nitrate hexahydrate and strontium nitrate anhydrous is added to the calcium nitrate solution such that the (Ca+Zn/Sr)/P ratio remains 1.67. Then the entire experiment is repeated as mentioned above. 2 mol%, 5 mol%, and 10 mol% zinc-doped and 2 mol% %, 5 mol%, and 8 mol% strontium-doped nanohydroxyapatite samples were synthesized. Pure and doped samples were denoted as HA, HAZn2, HAZn5, HAZn10, HASr2, HASr5, and HASr8 respectively.

Characterization

The structural analysis of the synthesized powder was done by powder X-ray diffraction. The X-ray diffraction pattern of the powdered

specimen is taken using Bruker D8 ADVANCE with DAVINCI instrument operating at 30 kV and 10 mA using Cu Kα radiation (λ=1.5418 Å). Diffraction patterns were collected over the range 10°≤ 2θ ≤79° with a step size of 0.02 ^{0}. The functional groups present in the sample were identified using FTIR spectrum. The FTIR spectra of prepared samples were recorded by Thermoscientific Nicolet iS50 instrument and recorded using the KBr pellet technique in the range 4000 - 400 cm^{-1}. The components in the sample were examined using EDX (Carl Zeiss EVO 18). The thermal stability was analyzed using thermogravimetric analysis (Perkin Elmer STA 8000). The morphology of the synthesized samples was determined by HRTEM analysis using Jeol/JEM 2100 instrument. The synthesized powder is pelletized using a hydraulic press at a pressure of 2.5 MPa and sintered to 1100^{0}C. The density of the sintered sample is determined using Archimedes' principle, and Vickers hardness was determined using Vickers hardness testing machine (Model-DVS-1AT-8) as per ASTM standard C1327-15. To determine hardness and density, pellets of 1 cm diameter and 2 mm thickness were used. Vickers hardness was measured for two samples at 5 different positions, and the average value was taken.

RESULTS AND DISCUSSION

XRD analysis

The XRD patterns for pure nanohydroxyapatite, as well as zinc-doped and strontium-doped variations, are presented in Figure 1. The XRD pattern of the examined samples can be indexed to the hexagonal crystal structure of hydroxyapatite (ICDD No. 09-0432). No additional peaks are found, which shows that the obtained powder is pure and only one phase is present. The d spacing for the most intense peak is found to be 2.822 A^0, which matches with that of the hexagonal system with a primitive lattice. The XRD pattern of zinc-doped hydroxyapatite is the same as that of pure hydroxyapatite, indicating that no additional crystalline phases are present. It has been observed that the peaks become wider and shift to higher angle values with the addition of zinc. This occurrence is due to the smaller ionic radius of zinc (0.74 Å) when compared with that of calcium (0.99 Å), along with the increased structural strain observed in zinc-doped hydroxyapatite compared to pure hydroxyapatite [7,8,20]. When zinc concentration increases, the crystallinity and crystallite size of hydroxyapatite decrease [8]. The presence of zinc in hydroxyapatite leads to the creation of crystal imperfections, resulting in a more defective hydroxyapatite crystal [8,16]. Doping hydroxyapatite with strontium (Sr) can result in an increase in the size of the crystallites, particularly at lower concentrations of strontium. This effect occurs because the ionic radius of strontium ions (Sr^{2+}, 1.18 Å) is larger than that of calcium ions (Ca^{2+}, 0.99 Å), which contributes to the expansion of the lattice [20]. Peaks become sharper and shift to lower angles due to strontium addition, due to reduced lattice strain and enhanced growth kinetics [11,14]. The size of the crystallites in the powder was calculated using the Scherrer equation, $D = \frac{0.9\lambda}{\beta \cos\theta}$. The broadened nature of diffraction peaks shows that the grain size of the sample was in the nanometer range. The crystallite size, lattice constants (a,c), cell volume, and crystallinity of pure and doped samples are given in Table -1.

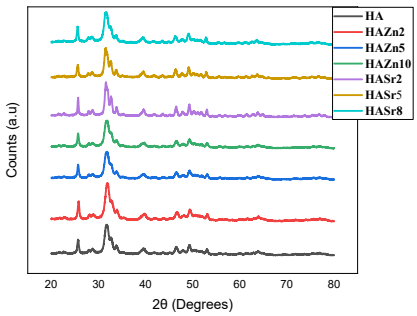

Figure 1 : XRD pattern of HA, HAZn2, HAZn5, HAZn10, HASr2, HASr5, and HASr8 samples

Table 1: The lattice constants, unit cell volume, crystallite size, and crystallinity of HA, HAZn2, HAZn5, HAZn10, HASr2, HASr5, and HASr8 samples

SL. No.	Sample	Lattice constants			Unit cell Volume(A^0)^3	Crystallite Size(nm)	Crystallinity
		a (A^0)	b (A^0)	c (A^0)			
1	HA	9.473	9.473	6.904	535.159	20.2	85.65%
2	HAZn2	9.453	9.453	6.891	533.318	20.12	81.34%
3	HAZn5	9.433	9.433	6.883	530.441	17.72	76.44%
4	HAZn10	9.432	9.432	6.882	530.298	17.5	75.90%
5	HASr2	9.474	9.474	6.912	537.350	22.11	85.21%
6	HASr5	9.479	9.479	6.917	538.332	22.31	84.43%
7	HASr8	9.485	9.485	6.921	539.370	22.41	84.02%

FTIR Analysis

The FTIR Spectra for pure, zinc-doped, and strontium-doped nanohydroxyapatite are illustrated in Figure 2. The distinctive bands of hydroxyapatite were detected in every sample, corresponding to phosphate, carbonate, and hydroxyl groups. The peak at 961 cm^{-1} was identified as characteristic of the symmetric stretching mode, v_1, of the PO_4^{3-} group, and that at 1021 cm^{-1} as the asymmetric stretching v_3 of the PO_4^{3-} group. The bending modes of phosphate group are seen at 600 cm^{-1} and 560 cm^{-1}, respectively, which refer to the O-P-O in-plane bending vibrations within the PO_4^{3-} group. The band at 3248 cm^{-1} corresponds to the -OH stretching vibrations of adsorbed water, while the peak at 630 cm^{-1} is due to the stretching vibrations of OH^- ions. The band corresponding to an asymmetric stretching of the CO_3^{2-} group occurs at 1420 cm^{-1} [7,8,18]. The FTIR analysis verifies the creation of hydroxyapatite, showing no presence of additional phases in the synthesized sample. The FTIR spectra demonstrate peak broadening and increased smoothness at elevated zinc concentrations, consistent with a reduction in crystallinity [18]. The shift in peak, attributable to strontium doping, consequently suggests carbonate substitution and lattice expansion [12-15].

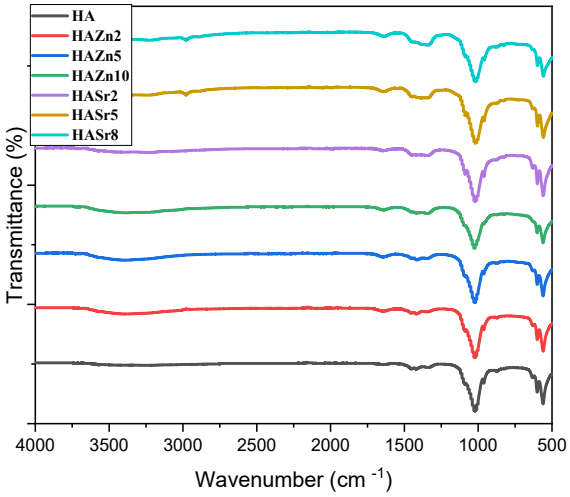

Figure 2 : FTIR spectra of HA, HAZn2, HAZn5, HAZn10, HASr2, HASr5, and HASr8 samples

Thermogravimetric analysis

The thermal stability of pure, zinc-doped, and strontium-doped nano-hydroxyapatite was studied using thermogravimetric analysis under a nitrogen environment in the temperature range of 30 ^{0}C - 800 ^{0}C. The graph is presented in Figure 3. A total mass loss of 8.35% is observed in pure hydroxyapatite in this temperature range. Three stages of degradation as a result of adsorbed and lattice water removal and de-hydroxylation of nano-hydroxyapatite were observed. These stages occur at 30 ^{0}C – 200 ^{0}C, 200 ^{0}C – 650 ^{0}C, and 700 ^{0}C – 800 ^{0}C, respectively. The first stage occurs due to the evaporation of physically adsorbed water from the hydroxyapatite surface. The second stage arises from the removal of chemically bound lattice water, decomposition of NO_3^{2-} groups, dehydration and condensation of HPO_4^{2-}, and crystallization of amorphous hydroxyapatite [21]. The third stage involves mass loss associated with decarbonization and dehydroxylation processes [8]. Zinc-doped hydroxyapatite shows a mass loss of 9.07%, 9.41%, and 14.85% for 2 mol% %, 5 mol%, and 10 mol% zinc-doped nano-hydroxyapatite in this temperature range. The weight loss increases with an increase in zinc concentration [5,17]. The thermal analysis indicated that the synthesized powders exhibit a certain level of thermal stability; however, this stability diminishes as the zinc fraction increases due to crystal deformation resulting from zinc substitution, which could facilitate the transformation from hydroxyapatite to TCP [8]. Strontium-doped hydroxyapatite shows a mass loss of 5.75%, 4.671%, and 3.38% for 2 mol%, 5 mol%, and 10 mol% strontium-doped nano-hydroxyapatite. The weight loss is minimum for strontium-doped hydroxyapatite because of its thermal stability. Findings show that moderate levels of zinc and strontium doping provide a balance between structural integrity and thermal resistance, which makes the sample suitable for biomedical applications [11,19].

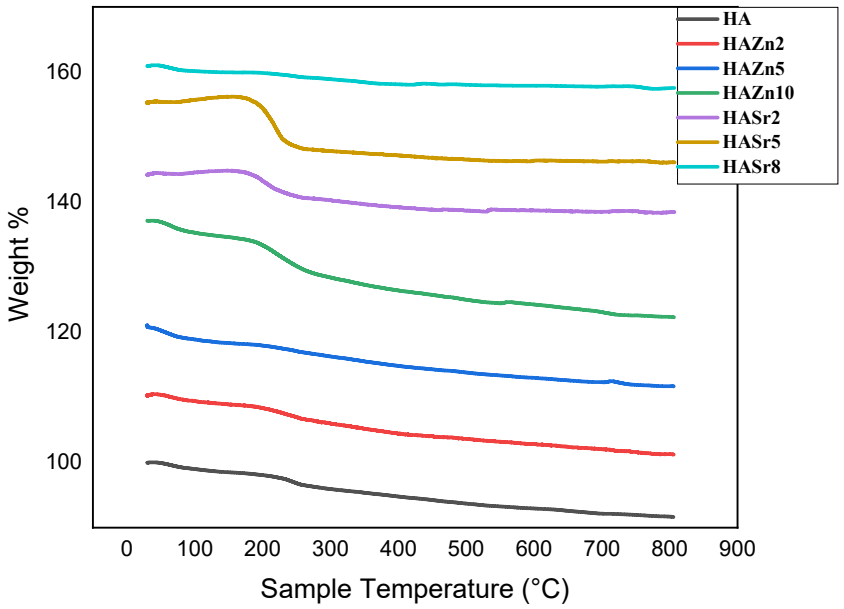

Figure 3 : Thermogravimetric curve of HA, HAZn2, HAZn5, HAZn10, HASr2, HASr5, and HASr8 samples

EDX Analysis

EDX analysis of HA, HAZn2, HAZn5, HAZn10, HASr2, HASr5, and HASr8 samples are shown in Figure 4. The Ca/P ratio for hydroxyapatite is found to be 1.72. When doping is done, the calcium-to-phosphorus ratio decreases, but the (Ca+Zn)/P or (Ca+Sr)/P ratio retains a value very close to 1.67. For HAZn 2, HAZn 5, and HAZn 10 samples, the (Ca+Zn)/P ratio is obtained as 1.74, 1.73, and 1.71, respectively. For HASr 2, HASr 5, and HASr 8 samples, the (Ca+Sr)/P ratio is 1.73, 1.76, and 1.72, respectively. All these values are very close to the theoretical value of 1.67. This analysis also confirms the successful incorporation of zinc and strontium in the sample.

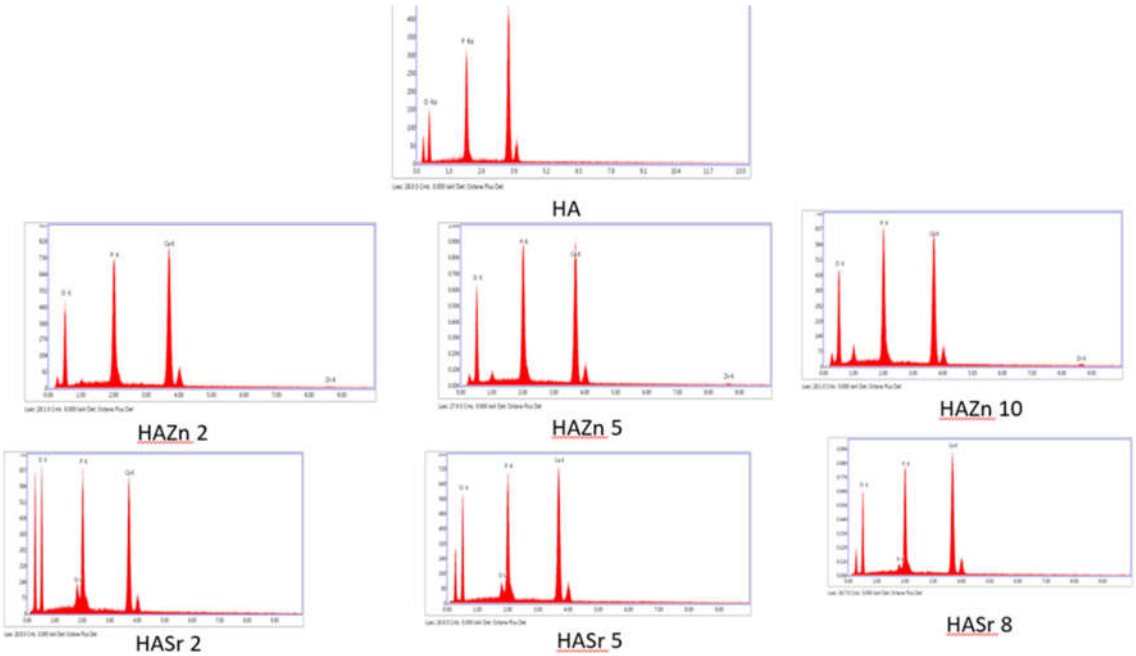

Figure 4 : EDX spectra of HA, HAZn2, HAZn5, HAZn10, HASr2, HASr5, and HASr8 samples

HRTEM Analysis

The HRTEM images of pure hydroxyapatite, 2 mol% zinc-doped, and 2 mol% strontium-doped hydroxyapatite samples are shown in Figure 5. Particles in all samples are found to be rod-shaped. The average particle size is found to be 31.53 nm, 41.04 nm, and 28.94 nm for HA, HAZn2, and HASr2 samples.

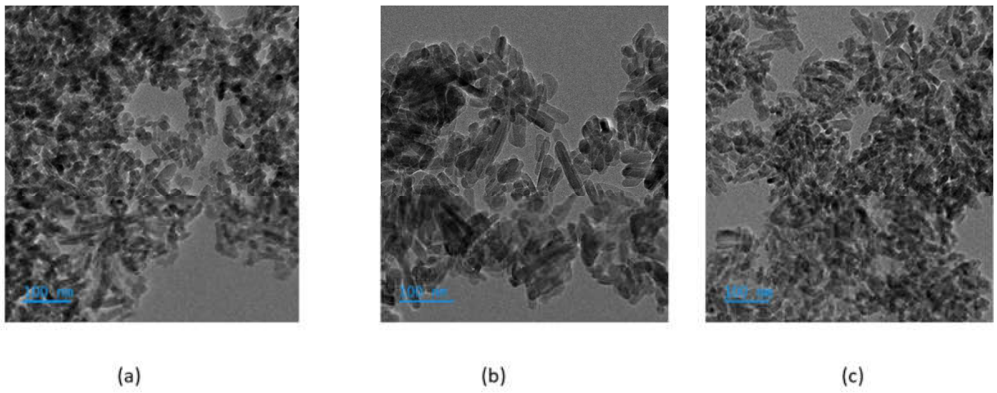

Figure 5 : HRTEM image of HA, HAZn2, and HASr2 samples

Density and Hardness

The density and Vickers hardness of the samples sintered at 1100 ^{0} C are given in Table 2.

Table 2 : Vickers hardness and density of HA, HAZn2, HAZn5, HAZn10, HASr2, HASr5, and HASr8 samples

Sample ID	Sintering temperature	Vickers hardness H_V	Hardness MPa	Density Kg/m ^{3}	Relative density (%)
HA	1100 ^{0}C	368.28	3612	2.27	71.83
HAZn2	1100 ^{0}C	416.5	4022	2.86	90.50
HAZn5	1100 ^{0}C	412.1	4038.58	2.72	86.08
HAZn10	1100 ^{0}C	410.15	4019.47	2.54	80.38
HASr2	1100 ^{0}C	436.98	4285	2.92	92.40
HASr5	1100 ^{0}C	402.56	3945.08	2.91	92.09
HASr8	1100 ^{0}C	391.1	3832.78	2.80	88.61

The density and hardness of the samples are found to increase with zinc and strontium doping at moderate levels. Due to improved grain packing, density increases for 2 mol% of zinc doping, and hence, hardness also increases. At 5 mol% % and 10 mol% of zinc doping density and hence hardness decreases due to the decomposition of hydroxyapatite and an increase in porosity [15]. For strontium doping, at 2 mol% strontium, density and hardness are found to be maximum due to enhanced diffusion and grain boundary mobility [15]. At 5 mol % and 10 mol% of strontium doping, density and hardness decrease due to the formation of secondary phases, leading to grain coarsening and increased porosity [15]. Hence, the optimum concentration of zinc and strontium doping is 2 mol% to get maximum density and hardness.

CONCLUSION

The current study successfully demonstrates the incorporation of zinc and strontium in hydroxyapatite. XRD and FTIR results confirm the incorporation of zinc and strontium in the sample. Thermogravimetric studies show that the sample becomes thermally stable due to strontium doping. For zinc doping thermal stability is the same as that of hydroxyapatite at low levels of doping, and it decreases for high levels of doping. EDX results also confirm the formation of hydroxyapatite and its doped samples. HRTEM results show the formation of rod-shaped particles, which are agglomerated. The sintered samples show enhanced density and hardness at low levels of doping. Future work should focus on the biological properties of optimized samples so that it can be used for various biological applications.

REFERENCES

1. Ingole, V. H., Ghule, S. S., Vuherer, T., Kokol, V., & Ghule, A. V. (2021). Mechanical properties of differently nanostructured and high-pressure compressed hydroxyapatite-based materials for bone tissue regeneration. *Minerals, 11*(12), 1390. https://doi.org/10.3390/min11121390
2. Sirajunisha, H., & Balakrishnan, T. (2017). Synthesis and characterisation of pure and doped hydroxyapatite nano powders by sol-gel method. *International Journal of Scientific & Engineering Research, 8*(10). https://doi.org/10.4236/jmmce.2011.108057
3. Weilin, Y., Tuan-Wei, S., Chao, Q., Zhenyu, D., Huakun, Z., Shichang, Z., Zhongmin, S., Ying-Jie, Z., Daoyun, C., & Yaohua, H. (2017). Evaluation of zinc-doped mesoporous hydroxyapatite microspheres for the construction of a novel biomimetic scaffold optimized for bone augmentation. *International Journal of Nanomedicine, 12*, 2293–2300. https://doi.org/10.2147/IJN.S126505

4. Ofudje, E. A., Adeogun, A. I., Idowu, M. A., & Kareem, S. O. (2019). Synthesis and characterization of Zn-doped hydroxyapatite: Scaffold application, antibacterial and bioactivity studies. *Heliyon, 5*, e01716. https://doi.org/10.1016/j.heliyon.2019.e01716
5. Senra, M. R., de Lima, R. B., de Holanda Saboya Souza, D., & Monteiro, S. N. (2020). Thermal characterization of hydroxyapatite or carbonated hydroxyapatite hybrid composites with distinguished collagens for bone graft. *Journal of Materials Research and Technology, 9*(4), 7190–7200. https://doi.org/10.1016/j.jmrt.2020.04
6. Mobasherpour, M., Soulati Heshajin, M., Kazemzadeh, A., & Zakeri, M. (2007). Synthesis of nanocrystalline hydroxyapatite by using precipitation method. *Journal of Alloys and Compounds, 430*(1–2), 330–333. https://doi.org/10.1016/j.jallcom.2006.05.018
7. Zhang, H., Zhao, C., Wen, J., L, X., & Fu, L. (2017). Synthesis and structural characteristics of magnesium and zinc doped hydroxyapatite whiskers. *Silikáty, 61*(3), 244–249. https://doi.org/10.13168/cs.2017.0022
8. Ullah, I., Siddiqui, M. A., Kolawole, S. K., Liu, H., Zhang, J., Ren, L., & Yang, K. (2020). Synthesis, characterization and in vitro evaluation of zinc and strontium binary doped hydroxyapatite for biomedical application. *Ceramics International, 46*, 14448–14459. https://doi.org/10.1016/j.ceramint.2020.02.242
9. Altomare, A., Mesto, E., Lacalamita, M., Dida, B., Mele, A., Bauer, E. M., Puzone, M., Tempesta, E., Capelli, D., Siliqi, D., & Capitelli, F. (2023). Structural characterization of low-Sr-doped hydroxyapatite obtained by solid-state synthesis. *Crystals, 13*(1), 117. https://doi.org/10.3390/cryst13010117
10. Hossain, M. S., Tuntun, S. M., Bahadur, N. M., & Ahmed, S. (2022). Enhancement of photocatalytic efficacy by exploiting copper doping in nano-hydroxyapatite for degradation of Congo red dye. *RSC Advances, 12*, 34080–34094. https://doi.org/10.1039/D2RA06294A
11. Bastan, F. E., Rehman, M. A. U., & Ustel, F. (2020). Thermo-physical insights into a series of strontium substituted hydroxyapatite. *Materials Chemistry and Physics*. https://doi.org/10.1016/j.matchemphys.2020.123910
12. Dapporto, M., Tavoni, M., Restivo, E., Carella, F., Bruni, G., Mercatali, L., Visai, L., Tampieri, A., Iafisco, M., & Sprio, S. (2022). Strontium-doped apatitic bone cement with tunable antibacterial and antibiofilm ability. *Frontiers in Bioengineering and Biotechnology, 10*, Article 969641. https://doi.org/10.3389/fbioe.2022.969641
13. Zhang, D., Zhang, H., Wen, J., & Cao, J. (2019). Preparation and characteristics of zinc and strontium co-doped hydroxyapatite whiskers. *IOP Conference Series: Earth and Environmental Science, 233*(2), 022007. https://doi.org/10.1088/1755-1315/233/2/022007
14. Tavares, D. d. S., Resende, C. X., Quitana, M. P., Castro, L. d. O., Granjeiro, J. M., & Soares, G. d. A. (2011). Incorporation of strontium up to 5 mol % to hydroxyapatite did not affect its cytocompatibility. *Materials Research. https://doi.org/10.1590/S1516-14392011005000073
15. Hadj Ali, R., Ageorges, H., Nasr, S., & Ben Salem, E. (2019). Zinc and strontium co-substituted hydroxyfluorapatite: Synthesis, sintering and mechanical properties. *Materials Research Bulletin, 112*, 84–94. https://doi.org/10.1016/j.materresbull.2018.11.042
16. Popa, C. L., Deniaud, A., Michaud-Soret, I., Guégan, R., Motelica-Heino, M., & Predoi, D. (2016). Structural and biological assessment of zinc doped hydroxyapatite nanoparticles. *Journal of Nanomaterials, 2016*, Article 1062878. https://doi.org/10.1155/2016/1062878
17. Abdel-Ghany, B. E., Abdel-Hady, B. M., El-Kady, A. M., Beheiry, H. H., & Guirguis, O. W. (2015). Characterizations of nano-zinc doped hydroxyapatite to use as bone tissue engineering. *Advances in Materials Research, 4*(4), 193–205. https://doi.org/10.12989/amr.2015.4.4.193
18. Venkatasubbu, G. D., Ramasamy, S., Ramakrishnan, V., Avadhani, G. S., Thangavel, R., & Kumar, J. (2011). Investigations on zinc doped nanocrystalline

hydroxyapatite. *International Journal of NanoScience and Nanotechnology, 2*(1), 1–23.

19. Ozbek, Y. Y., Bastan, F. E., & Ustel, F. (2016). Synthesis and characterization of strontium-doped hydroxyapatite for biomedical applications. *Journal of Thermal Analysis and Calorimetry.* https://doi.org/10.1007/s10973-016-5607-3
20. Nasiri-Tabrizi, B., Basirun, W. J., Yeong, C. H., & Thein, W. M. (2022). Development of the third generation of bioceramics: Doping hydroxyapatite with s-, p-, d-, and f-block cations and their potential applications in bone regeneration and void filling. *Ceramics International*.
21. Handa, S., Nath, D., Pal, A., & Sah, M. K. (2024). Biomimetic hydroxyapatite and strontium-doped derivatives from crab shells and their ingenious scaffold fabrication for bone tissue engineering. *Materials Today Communications.*

****